Chemistry Africa (2023) 6:629–642
https://doi.org/10.1007/s42250-023-00625-3

ORIGINAL ARTICLE

A Simple and Green Preparation Route of Waste Textile Based Photocatalytic Biochars for Pollution Removal

Huseyin Gumus[1] · **Bulent Buyukkidan**[2]

Received: 4 January 2023 / Accepted: 11 February 2023 / Published online: 27 February 2023

Abstract

The waste recycling is one of the smart methods to control the increasing demand for raw materials and environmental pollution. Photocatalytic biochars were prepared by carbonization of waste textiles that would not be reused in the industry. Virgin and $FeCl_2$, H_2SO_4, H_3PO_4 impregnated waste samples were carbonized at 300–400 °C for varying times. The functional groups and crystal structure of biochars were investigated by FT-IR and XRD respectively. SEM and BET analyzes were used to examine the morphology and surface properties of the biochars. $FeCl_2$ and H_3PO_4 impregnated samples presented well-crystalline and porous structure. Formation of functional groups increased at lower temperatures due to the catalytic effect. The highest dye removal by adsorption and photo catalytic effect were recorded as 25.65 mg/g and 97.8%, respectively. The order of efficiency for dye removal according to pretreatment was determined as $FeCl_2 > H_3PO_4 > H_2SO_4 >$ raw400 > raw350. Adsorbent-photocatalytic biochars were prepared by carbonization of chemically pretreated waste materials with a simple method. Environmental protection and economic production were achieved.

Graphical Abstract

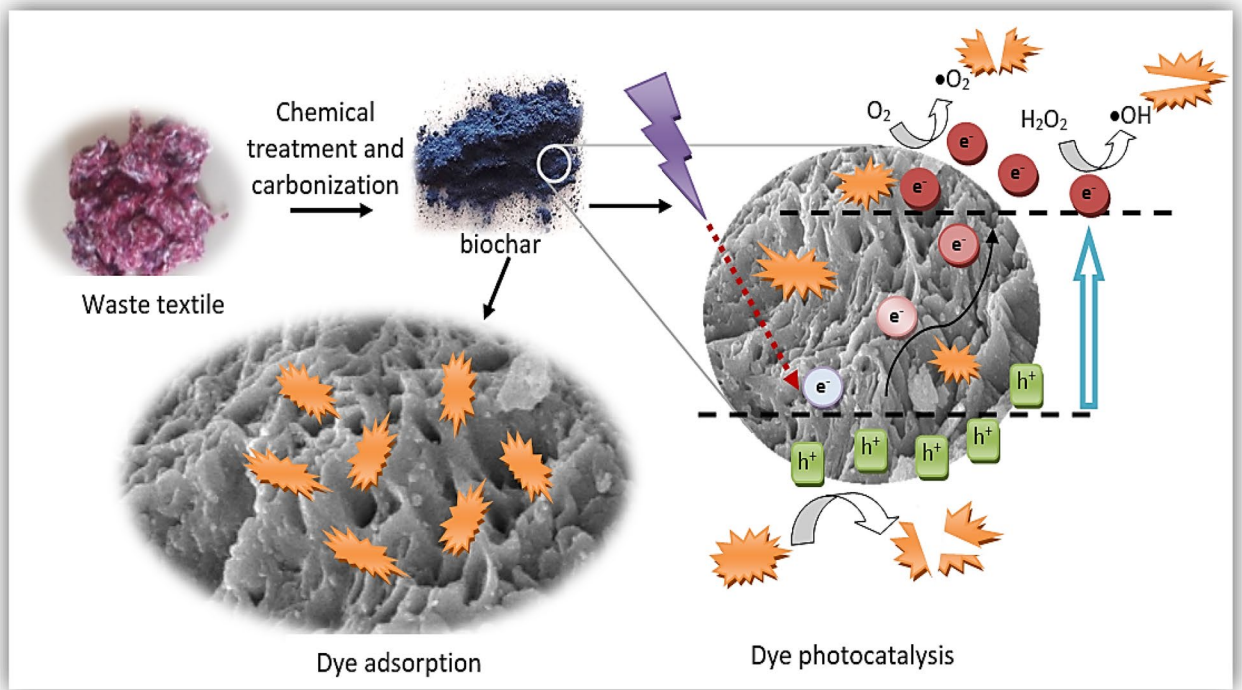

Extended author information available on the last page of the article

Keywords Adsorption · Biochar · Environmental protection · Photocatalysis · Recycling

1 Introduction

Most of the methods to obtain efficient carbon materials are based on general well-known techniques such as pyrolysis, hydrothermal carbonization, gasification, and torrefaction [1]. Various raw materials could be used for activated carbon. Different pyrolysis temperatures were investigated for rice straw and canola stalk at 450 °C. Among the applied temperatures 550–650 °C [2] was found as the best conditions to obtain high porosity and large pore sized activated carbon. Mangrove pile were exposed to different amount of H_3PO_4 and it was heated at 300, 400 and 500 °C [3]. Highest yield was obtained when the impregnation ratio of H_3PO_4: sample was 3. The AC3004 performed the best methylene blue removal (it was 72.3 mg/g at the 150 mg/L solution concentrations). The activated carbons having 976 and 1496 m^2/g surface area were prepared from bamboo and its solid by CO_2 activation [4]. KOH and $ZnCl_2$ pretreated waste truck tire and spent tea leaf were carbonized at 800 °C [5]. Polyvinylidene chloride resin was activated by ZnO at 950 °C [6]. Phosphoric acid and iron III chloride exposed carbonized coffee residue for bisphenol-A removal are the examples for different biochars obtained with different activation agents of various sources [7]. Rice husk, wheat straw, sawdust, sugar cane, cotton stalk, hemp stem, coconut leaf, corn corps, and bamboo are also some of the other biomaterials used for the preparation of activated carbon at different conditions such as activating agent, heating temperature, and time, etc.[8–12].

Functionalized active carbon could be obtained by modification of the sample with different methods. Thus, more effective adsorption, energy storage, and other applications could be achieved [13]. Used malt rootlets were simply dried and heated at 850 °C under limited air conditions. After that, it was exposed to sodium persulphate (SPS) at different concentrations to obtain a modified activated carbon catalyst. SPS modification dissolved inorganic and organic parts of the activated carbon and its surface properties changed with acidity. A functional-selective activated carbon was prepared by steam activation of commercial beech wood charcoal with K_2CO_3 [10] for deoxynivalenol (DON) removal. The particles of 8 µm sized with different pore volumes and pore sizes were obtained. The importance of tuned pore sizes was emphasized for 95% DON adsorption with 0.2 mg/ml adsorbent (at 37 °C and 1 h contact time). 23.48 mg/g xylene removal was achieved by palm kernel-based activated charcoal [11]. Activated carbons modified after simple preparation presented good catalytic and adsorption efficiency.

However, these multi-faceted preparation methods happen to have some disadvantages such as time, energy, and chemical consumption. Instead of that, the single-step preparation route could be more useful to be utilized. As it is known, activated carbon quality depends on parameters such as preparation method, temperature, biomass content, heating time, and pretreatment conditions. The chemical agent, amount, and pretreatment are significant importance to obtain activated carbon with desired properties. Acid–base and chemical pretreatment could be applied for the modification as well as separating the natural organic/inorganic matters. Many different methods for activated carbon preparation were reported for various biomass [14].

Wheat straw was used to prepare activated carbon by pretreatment and post-treatment with phosphate/magnesium agent. The pretreated sample presented the highest Pb^{2+} adsorption performance [15]. Brewers draff-based biochar (BCact) obtained at 650 °C was activated with 2 M KOH solution [16]. A small amount of increase for Cu^{2+} removal was recorded (10.3 mg/g whereas it was 8.77 for the non-activated sample).

The preparation of effective carbon-rich materials from biomass may be regarded as an economic route. Besides, converting carbon-rich waste into functional carbon-rich chemicals could provide a double effect, one of which is free of charge raw materials and the other one is preserving the environment. Fe (III) chloride impregnated waste cotton textiles could be a good example of triple benefit. It was concluded that the carbonization temperature of chemically treated samples was 163 °C whereas it was 300 °C for raw waste [17]. Fe (III) chloride treatment increased the CO_2 and H_2O releasing with decarboxylation. Obtained activated carbon presented 267.12 mg/g Cr (IV) removal performance. Mesoporous activated carbon with 1307 m^2 surface area was obtained by the carbonization of $MgCl_2$ pretreated waste polyester fabric at 900 °C [12]. Potassium salts of carboxymethyl cellulose for oil adsorption were synthesized by using purified wood wastes and cellulose-containing wastes of cotton cleaning factory [18]. Waste textile materials that could not be reused for weaving were used as unique biomass. Pretreatment, activation, and carbonization parameters are specific for only biomass that was handled.

Although adsorption is preferred due to its high efficiency and easy operation of confining the impurities on to porous surfaces, it does not signify the complete removal. In addition, desorption is required for the reuse of the adsorbent. The efficiency tends to decrease in reuse due to blocking of the adsorbent channels and deterioration inevitably. The

decomposition of adsorbed substrates into harmless components by an efficient mechanism is more interesting than simple adsorption. While the carbon rich structure ensures the adhesion of the substrate, an active agent integrated into this structure can catalyze the pollution. UV sensitive Fe_2TiO_5 modified biochar (Fe_2TiO_5/BC) was used to remove methylene blue with ultraviolet (365 nm and 100 W) irradiation [19]. It was predicted that methylene blue adsorbed on Fe-biochar and it interacted with reactive oxygen groups formed by ultraviolet light. Dye decomposed in accordance with the photo-fenton process. Effective hydroxyl radicals were formed by interaction of hydrogen peroxide with chitin biochar-ZnOFe_2O catalyst for Rhodamine-B (RhB) oxidation [20]. The oxidation of methyl orange (MO), methyl red (MR), methylene blue (MB) and different chemicals on the Ag containing magnetic biochar with $NaBH_4$ are some of the other examples for catalyst-doped-biochar applications [21, 22]. Active metal-biochar composites induce the formation of electron vacancies required for radical formation, electron transfer, and electron acceptor or donor. In addition, the metals in the structure physically strengthens biochar and affects adjusting pore formation and pore number. Carbonization of chemically pretreated biomass in one step seems to be easy, economic and environmental method to prepare light derived catalyst. The combination of carbon in Ag_3PO_4-MWCNT composite increased the stability and photocatalytic activity of the active catalyst thanks to the synergistic effect [23]. The rapid electron transmission of MWCNT on the photocatalyst surface could be done with biochars.

99% photocatalytic removal of MB and Congo red (CR) was achieved on the phosphate modified P-TiO_2/BC composite [24]. Need for 500 W lights is one of the disadvantages that reduces the system's efficiency. Biochar and carbon nanotube support were effective in removing 15 mg/L rifadin antibiotic in 150W UV, 50W Led irradiation of Ni–Cr photocatalyst. The carbon support increased the efficiency with its large surface area and electron transfer [25]. Considering the conditions of 50 mg of photocatalyst, 20–25 mg/L substrate for 1–4 h with 300–500 W power requisition, it would be beneficial to improve its feasibility.

Although some studies were carried out for dye adsorption performances of the chemically pretreated waste textiles based biochars, studies investigating the adsorption and photocatalytic performances of such biochars sequentially at lower power light (30 W) were not encountered in literature review.

This study aims to draw scientists' attention to the importance of specific treatments of biomass for functional activated carbon preparation. Therefore, cost-free waste textile materials that could not be reused in the textile industry were chemically pretreated and carbonized in a controlled manner. The effect of chemical treatment was investigated in terms of characterization techniques of SEM, BET, XRD, and FT-IR. The methyl orange (MO) model pollutant removal mechanisms of the samples were investigated in terms of adsorption and photocatalysis. Thanks to the optimum chemical pretreatment and carbonization method, a large porous biochar that could adsorb and catalyze impurities were synthesized. Energy requisition and other conditions were compared with the literature. A simple and green method was adjusted for the preparation of functional biochar from raw materials.

2 Experimental

2.1 Materials

Waste textile materials were obtained from Uşak Organized Industrial Zone, Turkey. C_2H_5OH, HCl, H_2SO_4, H_3PO_4, $FeCl_2.4H_2O$ were purchased from Sigma Aldrich and used without any processing. Methyl orange (from Sigma Aldrich) aqueous solution was used as an anionic model pollutant [26].

2.2 Preparation of Chemically Activated Biochars

Carbonization of waste textile remnants was conducted as above-mentioned. Waste textile samples were firstly washed with ethanol in 70–80 °C hot water to remove dirt and dye. It was dried at 60 °C for 24 h. 5 g sample was wetted by 25 ml activating H_2SO_4, H_3PO_4 or $FeCl_2.4H_2O$ agents. The mass ratio for activating chemicals: waste textile was adjusted to 0.14/1.4–50 for 1–1.5 h. The samples immersed in chemical were washed and dried at 60 °C oven for 24 h before the carbonization. Those were carbonized in a muffle furnace at 10–15 °C/min at the temperature ranges 350–400 °C. Static N_2 inert gas was infused in furnace before heating. Control samples were prepared by carbonization of textile samples at 350 and 400 °C without using any chemicals. Having been weighted and grounded, carbonized samples were passed through a 150 µm sieve. Prepared samples were called with explanatory determination in accordance with its activation procedure such as, [01/05/1]-[H2/H3/Fe]-[1/1.5]-[350/400] with H2, H3, Fe-CTW and CTW-350, CTW-400 abbreviations. 01/05/1 stands for the concentration of chemicals (mol/L) used for activation. H2, H3 and Fe represent the chemicals used for pretreatment. 1/1.5 and 350/400 are carbonization time (h) and carbonization temperature (°C) respectively.

2.3 Characterization of Biochars

Crystallinity and functional groups of prepared biochars were analyzed by XRD (Rigaku 2000) at $2\theta = 2–80°$ with

2°/min scanning speed and Perkin Elmer FT-IR over a range of 4000–400 cm^{-1}. Morphological images were pictured by scanning electron microscopy at 10 kV (Carl Zeiss ULTRA Plus). Surface area of biochars was measured by TriStar II 3020 Version 3.02 BET device. Concentration of initial and final dye solutions were analyzed by UV–visible spectrometer (Shimadzu, 2550) at 466 nm wavelength for MO. The mass loss (ML%) percentages of carbonized samples were calculated in order to determine carbonization process in accordance with Eq. (1)

$$ML\% = \frac{W_i - W_F}{W_F} \times 100 \quad (1)$$

W_i and W_F are initial and final mass (after carbonization) of textile samples, respectively.

2.4 Dye Removal Experiments by Adsorption and Photo Catalytic Effect

Dye removal performances of biochars were tested in a cylindrical flask by the batch technique. Adsorption temperature and pH of solutions was adjusted to 298–328 K and pH ≅ 7.0 respectively by 0.05 mol/L HCL and NaOH solutions. 100 mL MO aqueous solution (10–150 ppm) and 0.05 g adsorbent were put into adsorption cup, and stirred at 150 rpm for 90 min. In order to find out whether the dye removal mechanism is through adsorption or photo catalytic effect, the adsorption behavior of the samples before ultraviolet exposure was examined. The samples taken from the solution medium in 5 min were separated from the adsorbent by centrifugation and the amount of MO was analyzed by UV–vis spectrometer at 466 nm. As soon as each solution reached equilibrium, it was exposed to 30 W ultraviolet radiation for 35 min at a distance of 15 cm. Light intensity was adjusted ≅ 90 mW cm^{-2}. At the end of the 35th min, 10×10^{-5} mol/L hydrogen peroxide was added to the medium and exposed to UV for 5 more minutes. Thus, the dye removal efficiencies of biochars in adsorption, ultraviolet and hydrogen peroxide-ultraviolet environments were investigated. To verify the precision of experimental results, each part of the procedure was separately validated by repeating three times. Dye removal capacity (Q_e, mg/g) and efficiency (E_{AD}, %) of samples were calculated by Eqs. (2) and (3) for adsorption and photo catalytic process [27].

$$Q_e = \left(\frac{C_0 - C_e}{M}\right) \times V \quad (2)$$

$$E_{AD}(\%) = \left(\frac{C_0 - C_e}{C_0}\right) \times 100 \quad (3)$$

C_0 and C_e are initial and equilibrium dye concentration in mg/L respectively. M (g) and V (L) represent amount of adsorbent and the volume of MO solution.

3 Result and Discussion

3.1 Characterization of Biochars

The biochars prepared at [05]-[H2/H3/Fe]-[1]-[350] conditions with control samples obtaining at 350 and 400 °C were identified as the investigation samples. The samples were determined in terms of carbonization temperature, characterization results, and adsorption performances. The samples of CTW-350 and CTW-400 were prepared without any chemical. Carbonization efficiency decreased with the increasing temperature and 14% CTW-400 was obtained as least yield (Table 1).

The carbonization of waste textile did not complete at 350 °C. The high amount of the chemical treated samples

Table 1 Proximate analysis of CTW adsorbents

				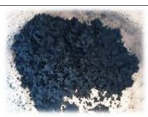	
Textile waste (TW)	CTW-350	CTW-400	Fe-CTW	H2-CTW	H3-CTW
Yield (%)	30	14	48	33	46
acidity (in aqueous solution)	neutral	neutral	acidic +	neutral-acidic	acidic
appearance and grinding	fragmentary, incomplete carbonization	well carbonized	Well carbonized, Iron oxide colored	Sticky structure due to acidic dissolution	Hardened structure, fragmentary

depend on the amount of activation chemical which adheres to the biochar structure. As could be understood from the color of samples, iron added biochar contains iron oxide species. Moreover, iron treatment induced the carbonization even at lower temperatures. Thus, well carbonized biochar was formed. Acid treatment did not increase the mass ratio of the carbonized product. Rigid structure of H2-CTW and H3-CTW could be partially seen from the images. Due to anti-burn effect of PO_4^{3-}, highly hardened H3-CTW was obtained. Therefore, the structure of H3-CTW prepared at 05-H3-1-400 conditions was almost similar to H3-CTW obtained at 350 °C due to fire retardant effect of phosphate groups [28].

The yields of acid treated waste consist of semi-carbonized samples with fragmentary structure. Due to solvent effect of H_2SO_4 on the waste textile, sticky and insufficiently carbonized materials formed. Before dye adsorption experiments, biochars were added to deionized water to determine their acidity. An interesting result was observed for water-Fe-CTW mixture, due to high acidity, while the others' pH was approximately neutral (pH 6.8–7.1). This situation might be the result of releasing the acidic species from the small amount of iron oxide reduction at the presence of carbon [29]. The content, activity, and yield percentage of carbonized samples could be adjusted as desired by scientific methods to obtain efficient adsorbents-catalyst.

The crystal structure patterns which pointed out the formation of biochar were presented in Fig. 1 for CTW-350, CTW-400, H2-CTW, H3-CTW and Fe-CTW.

Clear evidence for carbonization was observed for biochars obtained from both activated and non-activated waste. A broad peak among the 2θ = 15–30 could be attributed to characteristic crystalline structure of activated carbon [30]. Especially the peak at around 2θ = 25 became sharp for CTW-400 and H2-CTW with a small shift to lower angles. That implied to increasing crystallinity and increasing interspaces [31]. Some of the peaks such as 29.18°, 36.12° and 58° observed at Fe-CTW diffraction patterns are due to iron (II) oxide crystals formed as a result of Fe (II) cation impregnation [32]. According to XRD diffraction patterns, activation methods in this study could be classified as temperature, acidic and cationic induced. The crystallinity of biochars obtained by temperature induction competes with those obtained by chemical modification. CTW-350 and CTW-400

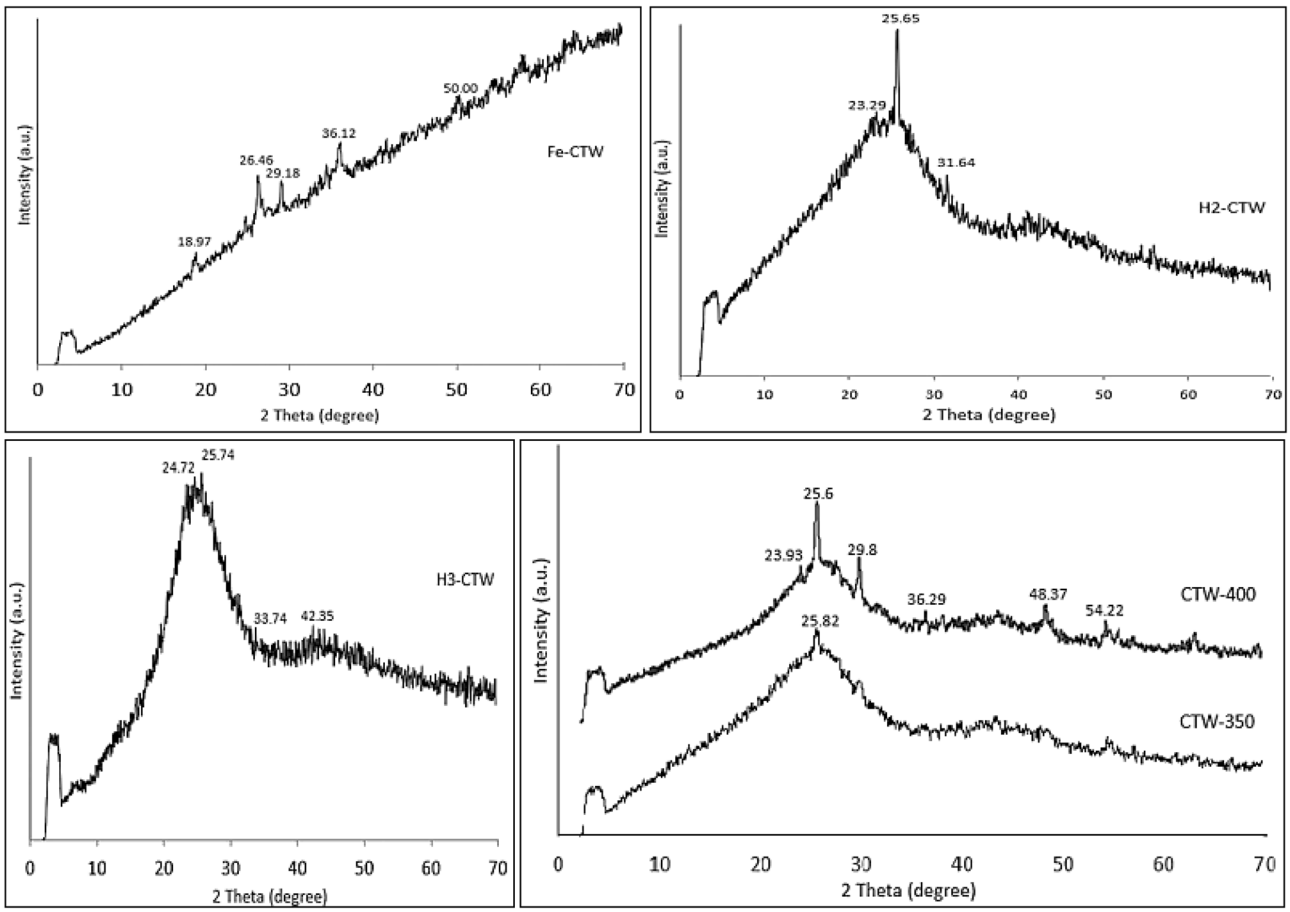

Fig. 1 XRD patterns of CTW samples

presented temperature differences for crystallinity while the others showed chemical effect. The broad peak shown on the H3-CTW diffraction pointed out the disordered structure and low crystallinity due to of large phosphate groups disrupting the crystal structure. The changes of chemical structure and functional groups were analyzed by spectroscopic analysis of FT-IR (Fig. 2).

From the spectrums of Fe, H2 and H3-CTW samples, characteristic carbonization peaks pointed out carbonization of cellulosic waste materials had been observed. The bands at around 3400, 1700 and 1090 cm^{-1} represent for OH, C=O and C–O–C vibrations respectively. The spectrum of non-activated CTW-350 and CTW-400 samples could be seen in our other study [33]. The band at around 1610 cm^{-1} was assigned to C=C bond stretching of aromatic ring, and it was observed for all samples [34]. The Fe activation resulted in different FeO formations on the Fe-CTW structure. That was inferred from the band at around 500–850 cm^{-1} with the 1083 cm^{-1} band that corresponds C–O–C vibration. The presence of different phosphate species could be understood from the clear 998 cm^{-1} bands of H3-CTW as much as the absence of 1700 cm^{-1} C=C band [35]. Surface morphology of obtained biochars is shown in Fig. 3.

The spongy-like surface of CTW-350 structure became a denser structure with the effect of temperature as could be understood from the CTW-400 surface. Despite increased temperature, the volatile matter of CTW-400 was not removed sufficiently due to melting of components in the

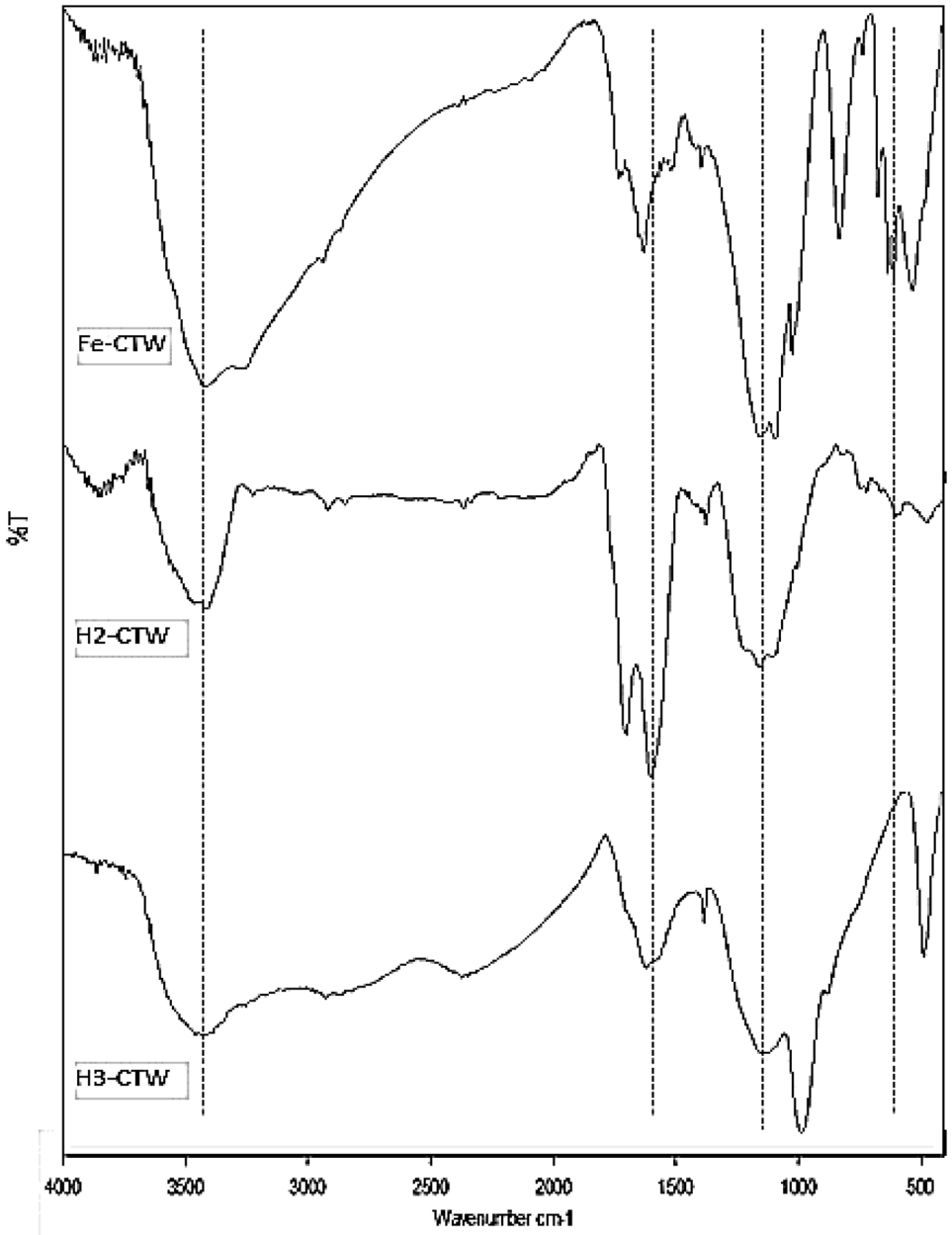

Fig. 2 FT-IR spectra of CTW samples

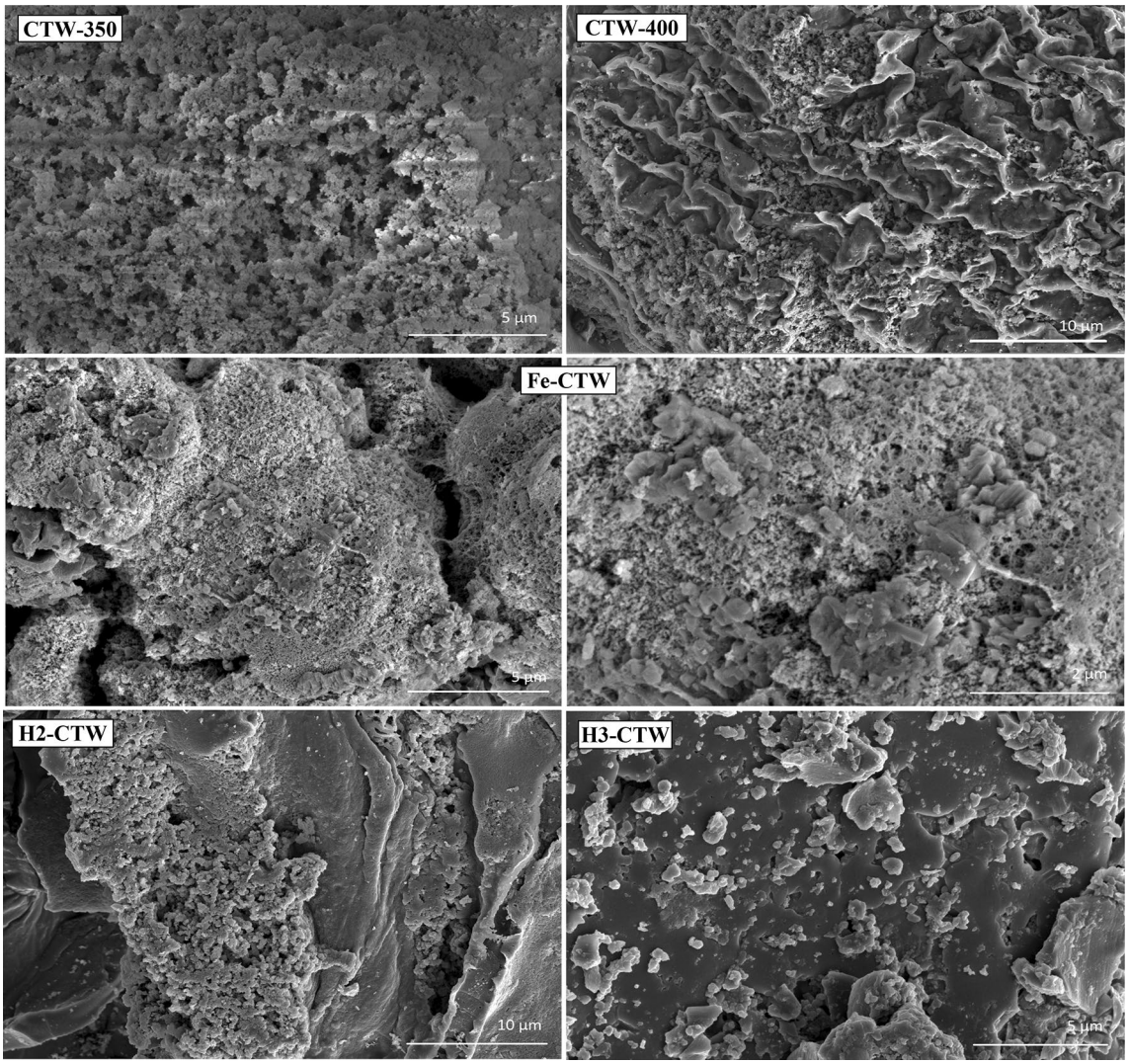

Fig. 3 SEM images of CTW samples

waste and it covered the biochar surface even at 400 °C. This indicated how important the temperatures with other parameters for sufficient carbonization. The crystal formations attributed to formation of iron oxide species with sponge-like structure were observed on the Fe-CTW image. Partially well-ordered pores and voids appeared in spite of lower carbonization temperature at 350 °C for Fe-CTW. Catalytic effect of iron species is considered as a dominant for transformation of active agents to substrate easily.

H2 and H3-CTW exhibited very dense structure compared with iron activated and non-activated samples due to solvent effect of acid on the waste materials. Thus, pores were covered with particles and chemicals dissolved during the pretreatment. Those penetrated to voids and depressed the pore formation. This effect could be understood from the BET results of the biochars (Table 2).

Table 2 BET surface area of (S_{BET}) CTW adsorbents

Sample	CTW-350	CTW-400	Fe-CTW	H2-CTW	H3-CTW
S_{BET} (m^2/g)	59	354	215	189	67

The largest surface was recorded for CTW-400 as 354 m^2/g while it was only 67 for H3-CTW. A well-ordered activated carbon with large pores was obtained with 4 ratio H_3PO_4 treated mangrove pile sample among 3–5 ratio and 300–500 °C temperature range in literature [3]. It is concluded that sufficient parameters should be determined for efficient carbonized yield by considering the waste material. The EDS analysis results revealed that carbon content reduced with increasing temperature and chemical treatment as shown in Table 3 and Fig. S1.

Table 3 EDS analysis results of CTW adsorbents

Atomic %	CTW-350	CTW-400	Fe-CTW	H2-CTW	H3-CTW
C K	82.98	70.49	53.39	85.95	52.11
N K	0.10	18.59	5.95	9.73	2.35
O K	11.40	2.70	29.28	3.18	23.64
MgK	3.14	7.64	0.60	1.14	0.07
AlK	1.56	0.36	10.77	85.95	17.47
SiK	0.26	0.22	–	–	0.86
TiK	0.54	–	–	–	3.50
FeL	–	–	14.04	–	–
P K	–	–	–	–	63.73

The catalytic effect of Fe species with decreasing carbon content compatible with explanations given at this section. On the other hand, reducing carbon amount of H3-CTW could be attributed to phosphate penetration to voids and interaction with volatile matters. Thus, carbon structure evaporates easily during the carbonization [3]. Presence of Fe and P atomic structure could be understood from the EDS graphs. That pointed out the formation of iron and phosphate species. Sulfuric acid was concluded as the minimal carbon reducing agent (with 85.95% carbon contents) for pretreatment of waste textile material. It was probably dissolution of waste textile samples with the effect of sulfuric acid rather than exchange or elimination of carbon content. The highest carbon content was obtained in CTW-350 and CTW-400 respectively proportional to the applied temperature.

3.2 Dye Removal by Adsorption and Photo Catalysis

3.2.1 Adsorption Properties

It was investigated whether the dye removal performances of the prepared biochars were through adsorption or photocatalysis. In order to actualize that, 100 mL of MO (10–150 ppm) solution and 0.05 g adsorbent were put into adsorption cup, and stirred at 150 rpm for 90 min. Solution pH was adjusted to: 7, before adsorption. This pH value was chosen considering the anionic character of the model pollutant and the approximately neutral pH of MO aqueous solution (≅7.23). The anionic structure of MO has a facilitating effect on the cationic adsorbent for adsorption (Table S1). However, the change in the active groups of the solid (surface charge) in acidic medium is vital importance. Increasing the positive charges on the adsorbent surface will increase the MO adhesion. Anionic stability of dye in an acidic environment is also another important factor. The adsorption of MO at different pH values is the subject of other studies. Since the adsorption and photocatalytic effect were investigated sequentially, the pH of the MO solution was used directly at neutral pH value, excluding the different pH effect. Temperature effect was studied at 308, 318, and 328 K, however any remarkable increase was not observed for MO adsorption. So, 298 K was decided as adsorption temperature for this study. During the photocatalytic process, the ambient temperature was kept at the determined constant value with controlled cooling. The adsorption performances of biochars in batch media were examined by UV spectrometer taken 1 mL samples at regular intervals for 90 min. Afterwards, the solution was exposed to ultraviolet irradiation (30 W) for 35 min in air circulation and for 5 min in the presence of 0.01 mol/L H_2O_2 consequently. Thus, the dye removal performances of biochars were investigated in terms of adsorption and photocatalytic effects.

Adsorption on biochar is a widely preferred method for removing impurities in aqueous media. However, the cost of the material and the process type are the parameters that directly affect the efficiency. Since this study focuses on the preparation of biochar with high dye removal by simple methods, the photocatalytic sensitivities of the samples were investigated besides their adsorption performance. Dye removal efficiencies of biochars were tested under basic and least costly conditions consisting of approximately neutral MO solution, 298 K temperature, 0.05 g adsorbent, 35 min air and 5 min H_2O_2, Fig. 4.

The CTW-400 and H3-CTW samples showed increased MO removal compared to the others. The adsorption efficiency of Fe-CTW and H2-CTW started to decrease after the 45th min and after the 75th min of the CTW-350. These changes reveal the direct dependence of adsorption on surface properties of biochars. Satisfactory dye removal efficiency of CTW-400 can be explained by its large surface area. The low surface area of CTW-350 with only temperature variable biochar resulted in low adsorption. However, it is understood from both MO adsorption and characterization results that the adsorption efficiencies of biochar prepared without chemicals at 400 °C (CTW- 400) provide moderate adsorbent properties. Although the gap between the surface areas of CTW-400 (354 m^2/g) and H3-CTW (67 m^2/g) is very large, the high adsorption efficiency recorded in H3-CTW is due to the presence of functional groups on the surface. Its performance gradually increased and a dye removal efficiency of 96.4% was recorded at 90th min. It greatly exemplifies the possibility that more efficient adsorbents containing functional groups can be obtained at low temperature through chemical treatment. Although Fe-CTW and H2-CTW were obtained by chemical treatment, they presented low adsorption efficiency. That can be explained by small pores formed most of their large surfaces prevent MO entrance partially. The proper voids and pores that formed on the adsorbent surface after the chemical treatment provided higher adsorption. It is understood from the results that the large surface area alone is not sufficient to achieve high adsorption. The proper pore diameters and the

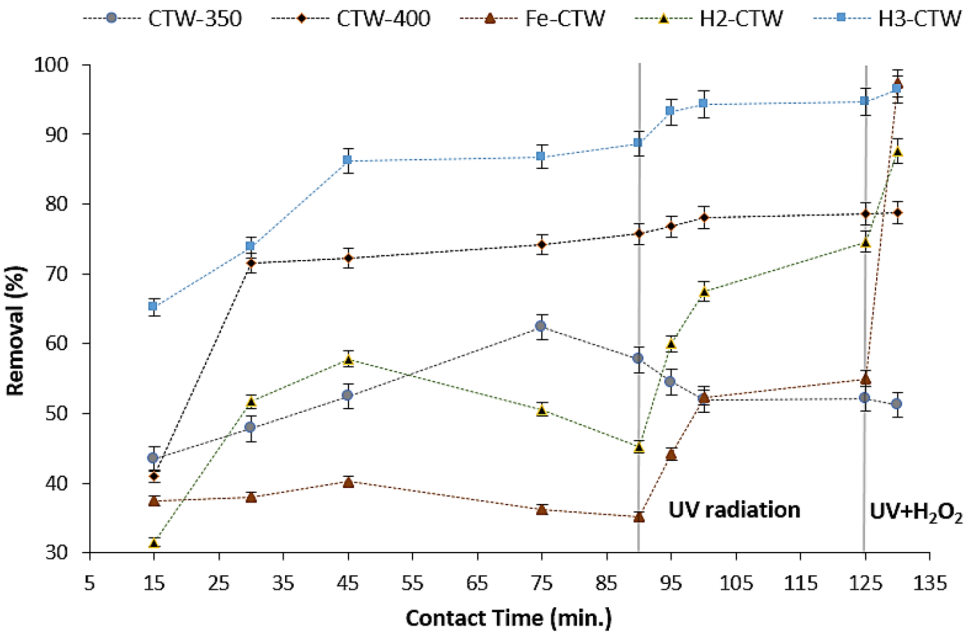

Fig. 4 MO removal (%) performances of biochar (adsorbent dosage: 50 mg, dye concentration and volume:75 mg/L, 100 mL, pH:7.23, temperature: 298 K, 30 W UV radiation for 35 min (after the 90th min) and, 30 W UV radiation for 5 min with 0.01 mol/L (after the 125th min)

functional groups on the adsorbent surface are of undeniable importance and, Fe-CTW and H3-CTW were concluded to present these functional groups. On the other hand, adsorption performance of H2-CTW was less than the expected correlation with others. The solubility of raw waste textile content particularly with a high percentage of cotton in H_2SO_4 resulted in preventing effect for the appropriate carbonization. Acid treated samples was covered with sticky slush and that increased during the carbonization. This structure prevented the efficient carbonization and formation of functional groups and pores. It is important to note that, a procedure for carbonization is specific for a handled raw material even if it was the similar content.

The adsorption data versus time were applied to the Langmuir and Freundlich isotherms to better understand the adsorption mechanism [26, 33, 36] (Table S2 for equations of isotherms and kinetic).

At this point, C_e (mg/L), which is the MO concentration in the aqueous solution after adsorption, and Q_{max}, which is the maximum monolayer adsorption capacity of the sorbent. K_f and K_L, are the constants of the Langmuir and Freundlich model isotherms, respectively. Adsorption isotherms are important in terms of providing information about the adhesion mechanism of dye molecules on the adsorbent surface. Relying on the consistency of the related graphics, it can be predicted whether the adhesion occurs as a single layer on a homogeneous surface or a single or multiple layer on a heterogeneous surface. The adsorption parameters were presented in Table 4.

MO adsorption on the biochars could be explained by Langmuir and Freundlich isotherms in generally. While the values of CTW-350 and CTW-400 are suitable to be explained by Freundlich isotherm, MO adsorption on biochars prepared with chemical pretreatment can be explained by Langmuir model in Fig. S2.

It is understood that the MO adsorption on the CTW-350 and 400 complies with the multilayer adsorption mechanism on the heterogeneous surface. The adsorption on the Fe, H3 and H2-CTW can be explained by the monolayer homogeneous adsorption mechanism. The adsorption behavior of biochars is compatible with their structural differences. The maximum adsorption capacity was calculated as 59.17 and

Table 4 Isotherm and pseudo first order kinetic parameters of biochars for MO adsorption

	Langmuir isotherm			Freundlich isotherm			Pseudo-firs order kinetic			
	Q_{max} (mg/g)	K_L (L/mg)	R^2	K_f ($mg^{1-n}/g\ L^n$)	1/n	R^2	$Q_{e.exp}$	k_1	$Q_{e.cal}$	R^2
CTW-350	34.36	0.01275	0.9541	1.31	0.7078	0.9747	15.11	0.083	14.54	0.977
CTW-400	59.17	0.01377	0.9602	14.43	0.7066	0.9769	26.87	0.113	25.82	0.978
Fe-CTW	43.29	0.0181	0.981	1.42	0.6572	0.9664	37.01	0.057	32.17	0.725
H3-CTW	51.28	0.0186	0.9711	1.79	0.6439	0.9741	25.4	0.1	24.61	0.988
H2-CTW	23.58	0.01766	0.9976	1.13	0.6194	0.9811	20.41	0.031	17.21	0.81

51.28 mg/g for CTW-400 and H3-CTW respectively, under the different MO concentrations. Considering the percentages of dye removal efficiencies, the values calculated for the low-cost adsorbents are quite reasonable. In addition, the data obtained from the Freundlich equation shows the adsorption of MO on the heterogeneous surface of CTW-400. In this context, $n > 1$ value can be interpreted as heterogeneous surface efficiency is higher than homogeneous surface.

Therefore, in accordance with the literature, it is understood that the adsorption of MO usually fits both Langmuir and Freundlich isotherms [28, 33]. The small differences of isotherm models indicate that MO adsorption fits both monolayer on homogeneous surface and multilayer on heterogeneous surface rather than a uniform model. Ouedrhiri et al. exemplified that the maximum MO adsorption values on biochar samples prepared from different raw materials at 298 K temperature were in a wide range such as 18.8–461 mg/g [37]. The MO removal efficiencies of biochars prepared under very economic conditions are consistent and satisfactory with the literature data. The adsorption efficiencies of all biochars at different initial MO concentrations and optimal conditions are promising.

3.2.2 Photocatalytic Activity

The adsorption of MO for 90 min, and the change in the amount of MO in the presence of UV light, is given in Fig. 4. The contact time of 45 min was decided to be the optimum value for adsorption of MO on all samples except H3-CTW and CTW-400. The decrease in MO removal percentage with increasing contact time, was due to MO desorption. But, the MO amount in the aqueous solution containing H2-CTW and Fe-CTW decreased with UV exposure after desorption. Increased MO removal clearly indicates that the photocatalysis of MO in the case of UV is not because of new adsorption.

Adsorption and photocatalysis were carried out sequentially in order to understand the removal of dye is caused by free radicals that form on the surface of catalyst [38]. When photocatalysis were applied separately, the solution and biochars were mixed in the dark for 45 min before reaching the equilibrium. The highest increase in MO% removal in the presence of UV was recorded as 62.7% on the Fe-CTW surface. This was followed by H2-CTW with 42.3% and H3-CTW with 7.7%. Desorption tendency of CTW-350 and CTW-400 in the UV conditions are proof that these structures provided no photocatalytic activity. The MO adsorption on CTW-400 remains constant in the presence of UV. It increased for CTW-350 as a result of MO desorption from the CTW-350 surface. The increase in the amount of MO at the CTW-350 solution also shows that MO remains unaffected even in the presence of UV light and peroxide. This proves the need for the use of an effective photosensitive catalyst for photocatalytic dye removal as well as UV light and oxidizers. There was no change in the MO concentration exposed to UV in the absence of any catalyst as a control experiment.

Different mechanisms are suggested for the removal of organic pollutants with the formation of radiation induced radicals, using different light absorbents. In these processes, which usually proceed over the electron–hole pair, the valance band electron of the catalyst exposed to the beam is excited to the conduction band. That results in valance gap (h^+) and conduction band electron (e^-). This is followed by the conversion of oxide, hydroxide, or peroxide derivatives in the reaction medium into radicals which catalyze organic impurities (Eqs. 4–9). If radical formation is provided by the iron catalyst in the presence of radiation, this reaction is called the photo-Fenton process [39, 40].

$$\mathrm{Fe/H2/H3-CTW} + h\nu \rightarrow e^- + h^+ \tag{4}$$

$$Fe^{2+} + H_2O_2 \rightarrow Fe^{3+} + {}^{\cdot}OH + OH^- \tag{5}$$

$$H_2O + h^+ \rightarrow {}^{\cdot}OH + H^+ \tag{6}$$

$$O_2 + e^- \rightarrow O_2^{-\cdot} \tag{7}$$

$$H_2O_2 + h\nu \rightarrow 2{}^{\cdot}OH \tag{8}$$

$${}^{\cdot}OH + \mathrm{dye} \rightarrow \mathrm{dye_{ox}} \tag{9}$$

When the MO removal efficiencies of Fe-CTW in different oxygen sources are compared, it was seen that the efficiency in the presence of peroxide increased by 43.7% compared to that of in the air circulation. Examination of MO removal in the presence of air and peroxide provided a better determination of the tendency of biochars to form radicals in the radiation. The high photocatalytic activity of Fe-CTW despite its small pore structure indicates that the reaction may proceed in the direction of providing radicals to the solution rather than the elimination of MO on the biochar surface. A slight increase in the MO removal was noted for H2-CTW and H3-CTW in the presence of peroxide. This revealed the distinction between adsorption-based and photo-induced dye removal as soon as better understanding the effect of peroxide. This study aims to prepare light sensitive biochars at low cost and to reveal their photocatalytic activities. Another advantage of Fe-CTW is the absence of Fe^{2+} release into the solution medium. In Fenton processes, Fe^{2+} and H_2O_2 added directly to the aqueous medium interact and the Fe-hydroxyl precipitation may cause the reaction to proceed uncontrollably and create separation difficulties. Biochar not only facilitates photocatalysis on the surface

with MO adsorption but also prevents metal leaching. Good adsorption is essential for highly productive photocatalysis. Large surface area and pores large enough to trap the adsorbent may increase adsorption ratio. The biochar obtained from the chemically treated carbon source allows the adjustment of the desired pore structure. At the same time, the active metal-large surface area couple provided an efficient photocatalyst [41–43]. MO removal activities of biochars were applied to pseudo first order and pseudo second order kinetic models. The Q_t versus time data for CTW-350, CTW-400 and H3-CTW performed the kinetic model, but the highest Q_e value was calculated for Fe-CTW. The rapid increase in MO removal, which is an indicator of the photocatalytic activity of Fe-CTW and H2-CTW, reduced the compliance with kinetic model (Fig. S3). C_0 (mol/L), C_t and k (min^{-1}) represent the MO concentrations for initial and at time t with the rate constant respectively. The rate constant 0.057 min^{-1} calculated for the Fe-CTW is consistent with the literature data. The photocatalytic activity of H2 and H3-CTW is very interesting and beneficial. The catalyst formed as a result of the addition of H_2SO_4 to TiO_2, ZrO_2, Al_2O_3 derivatives showed increased efficiency in NO_2 removal thanks to the sulfate derivatives that increase the active surface oxygen [41]. In addition, the surface acidity of the catalyst was increased by SO_2 treatment in order to increase the surface sulfate oxides. Thus NO removal efficiency increased in the presence of NH_3 on CeO_2 [42]. CeO_2-P and CeO_2-S refer to Ce catalysts containing phosphate and sulfate groups, and these groups were reported to increase the defect sites of the catalyst, called oxygen vacancy [42]. As seen in these examples, phosphate and sulfate groups are added to the catalyst at the synthesis stage or afterwards to increase the surface acidity or oxygen vacancies. Thereby the catalyst efficiency increases with a synergistic effect. The role of phosphate and sulfate groups in photocatalysis is quite evident, since photocatalytic reactions proceed through the formation of electron vacancies with the effect of photons. H2-CTW and H3-CTW prepared in this study are the examples of biochar-SO_2 and biocahar-PO_3 couples respectively. The MO% removal of these samples is the result of the photocatalytic activity. Photocatalysis of MO with Fe-CTW according to the fenton process is compatible with reactions using iron oxide derivatives [43]. H2, H3 and Fe-CTW compounds prepared by treating only certain chemicals offer a good cost-effective option. On the other hand, biochars provided physical and conductive support affect these metal–metal oxide groups.

Many studies have been reported on the adsorption and catalytic removal of dye, organic pollution and heavy metals using biochar-metal composition [46]. The removal rates of the adsorbent/catalyst used in the study, application conditions, preparation steps, substrate type and cleaning methods are the proofs of the success of the application. Different dye removal studies under similar conditions are given in Table 5 for comparison.

It is understood that the Fe-CTW, H2-CTW and H3-CTW biochars prepared in this study require very low energy compared to their counterparts for their remarkable photocatalytic efficiency. In addition, their preparation under low energy and chemical conditions using waste textile are the factors that enhance the preferability of the composites. Double benefit obtained with the converting the waste textiles by chemical treatment and controlled carbonization to metal–carbon material. One of them is the production of fine chemicals from cost free raw materials with an economical route and the other one is controlling the environmental pollution caused by disposal or burning of waste materials.

Table 5 Photocatalytic dye removal studies with different adsorbent-photocatalyst

Catalyst-Biochar precursor	Amount	Substrate and amount	Power (W)	Time	Removal mechanism and efficiency	References
pCN/WFB/Bi-VO_4 (Wood flour based)	50 mg	10 mg/L Rhodamine B	400–200	30 min	Degradation 97.3%	[44]
ZnFe-BC (poplar saw dust based)	0.04 g	Rhodamine B 25–35 mg/g and malachite green 80–120 mg/g	Unknown	180 min	Degradation 99.05% and 98.08%	[45]
Switch grass	2 g/L	2.5–320 mg/L Orange G	–	15 min–24 h	Adsorption 38.8 mg/L	[46]
ZnO/biochar (bamboo based)	100 mg	160 mg/L methylene blue	250	≅200 min	Degradation 95.19%	[47]
TiO_2-biochar (waste walnut shells based)	10 mg	20 mg/L methyl orange	500	150 min	Degradation 96.98%	[48]
Fe-CTW H2-CTW H3-CTW ($FeCl_2$, H_2SO_4 and H_3PO_4 treated Waste Textile based) biochar	50 mg	75 mg/L methyl orange	30 W	35 + 10 min	Degradation* 87.4% 77.6% 98.4%	This study

*Stirred for 45 min to reach adsorption equilibrium

4 Conclusions

Processing of industrial waste provides free of charge raw material besides environmental protection. In this study carbon-rich waste textile materials were handled in terms of active carbon preparation process. $FeCl_2$, H_2SO_4 and H_3PO_4 pretreatment methods were applied to acquire more functional and energy saving carbonization. Samples pretreated with activating agents were carbonized at 350 °C. The heating at 400 °C was necessary to obtain minimal features biochar from nonchemical-treated waste as control sample. The structure of biochars was analyzed with FT-IR, SEM, XRD and BET investigations. Some functional groups, porous structure and large surface area were observed at chemical treated samples. The dye removal of the biochars by adsorption and photocatalysis was sequentially investigated. The UV sensitivity of the Fe, PO_4 and SO_4 groups were understood from their performance in MO removal. The samples of Fe-CTW and H3-CTW were concluded as convenient adsorbent-photocatalyst that obtained with 05-Fe/H3-1-350 carbonization conditions. The highest MO removal performances of biochars by either adsorption or photocatalyst were recorded as 25.65 mg/g and 97.8% respectively. These results were highly acceptable if the dye removal performances of commercial or lab scale biochars at application conditions are taken into consideration. All carbon-rich materials could be converted to fine chemicals that could be used for adsorbent, biosensor or charging materials. However, the most feasible conditions should be scientifically determined. Waste textile materials were converted to activated carbon with cationic and acidic pretreatment and functional Fe-CTW, H2-CTW and H3-CTW were prepared with lower energy. These findings contain promising result for waste management aimed environmental protection and production of fine chemicals with economically.

Supplementary Information The online version contains supplementary material available at https://doi.org/10.1007/s42250-023-00625-3.

Acknowledgements We would like to thank the Chemistry Department of the University of Kutahya Dumlupinar for their support in providing the laboratory equipment.

Funding This work was financially supported by the Department of Scientific Research Project at the University of Kutahya Dumlupinar (DPÜ-BAP No: 2020-08).

Data availability The data of these study are available to download from [https://data.mendeley.com/datasets/h6k6k37m9r].

Declarations

Conflict of Interest The authors declare that they have no conflicts of interest.

References

1. Yaashikaa PR, Kumar PS, Varjani S, Saravanan A (2020) A critical review on the biochar production techniques, characterization, stability and applications for circular bioeconomy. Biotechnol Rep 28:e00570. https://doi.org/10.1016/j.btre.2020.e00570
2. Yang C, Liu J, Lu S (2021) Pyrolysis temperature affects pore characteristics of rice straw and canola stalk biochars and biochar-amended soils. Geoderma 397:115097. https://doi.org/10.1016/j.geoderma.2021.115097
3. Zakaria R, Jamalluddin NA, Abu Bakar MZ (2021) Effect of impregnation ratio and activation temperature on the yield and adsorption performance of mangrove based activated carbon for methylene blue removal. Res Mater 10:100183. https://doi.org/10.1016/j.rinma.2021.100183
4. Khuong DA, Nguyen HN, Tsubota T (2021) Activated carbon produced from bamboo and solid residue by CO2 activation utilized as CO2 adsorbents. Biomass Bioenergy 148:106039. https://doi.org/10.1016/j.biombioe.2021.106039
5. Guclu C, Alper K, Erdem M, et al (2021) Activated carbons from co-carbonization of waste truck tires and spent tea leaves. Sustain Chem Pharm 21:100410. https://doi.org/10.1016/j.scp.2021.100410
6. Hwang B, Yi SH, Chun SE (2021) Dual-role of ZnO as a templating and activating agent to derive porous carbon from polyvinylidene chloride (PVDC) resin. Chem Eng J 422:130047. https://doi.org/10.1016/j.cej.2021.130047
7. Naganathan KK, Faizal ANM, Zaini MAA, Ali A (2021) Adsorptive removal of Bisphenol a from aqueous solution using activated carbon from coffee residue. Mater Today Proc 47:1307–1312. https://doi.org/10.1016/j.matpr.2021.02.802
8. Sime T, Fito J, Nkambule TTI et al (2023) Adsorption of congo red from textile wastewater using activated carbon developed from corn cobs: the studies of isotherms and kinetics. Chem Afr. https://doi.org/10.1007/s42250-022-00583-2
9. Lokteva ES, Golubina EV, Antonova MV et al (2015) Chlorobenzene hydrodechlorination catalyst prepared via the pyrolysis of sawdust impregnated with palladium nitrate. Kinet Catal 56:764–773. https://doi.org/10.1134/S0023158415060099
10. Müller BR (2021) Preparation and characterization of K2CO3-doped powdered activated carbon for effective in-vitro adsorption of deoxynivalenol. Bioresour Technol Rep 15:100703. https://doi.org/10.1016/j.biteb.2021.100703
11. Pazira R, Lashanizadegan A, Sharififard H, Darvishi P (2018) Xylene removal from dilute solution by palm kernel activated charcoal : Kinetics and equilibrium analysis Advances in Environmental Technology Xylene removal from dilute solution by palm kernel activated charcoal : Kinetics and equilibrium analysis. Adv Environ Technol 2:83–92. https://doi.org/10.22104/AET.2018.2989.1145
12. Yuan Z, Xu Z, Zhang D et al (2018) Mesoporous activated carbons synthesized by pyrolysis of waste polyester textiles mixed with Mg-containing compounds and their Cr(VI) adsorption. Colloids Surf, A 549:86–93. https://doi.org/10.1016/j.colsurfa.2018.04.008
13. Minceva M, Markovska L, Meshko V (2007) Removal of Zn2+, Cd2+ and Pb 2+ from binary aqueous solution by natural zeolite and granulated activated carbon. Maced J Chem Chem Eng 26:125–134
14. Cuong DV, Matsagar BM, Lee M et al (2021) A critical review on biochar-based engineered hierarchical porous carbon for capacitive charge storage. Renew Sustain Energy Rev 145:111029. https://doi.org/10.1016/j.rser.2021.111029
15. Miao Q, Li G (2021) Potassium phosphate/magnesium oxide modified biochars: Interfacial chemical behaviours and Pb binding

performance. Sci Total Environ 759:143452. https://doi.org/10.1016/j.scitotenv.2020.143452
16. Trakal L, Šigut R, Šillerová H et al (2014) Copper removal from aqueous solution using biochar: effect of chemical activation. Arab J Chem 7:43–52. https://doi.org/10.1016/j.arabjc.2013.08.001
17. Xu Z, Sun Z, Zhou Y et al (2019) Insights into the pyrolysis behavior and adsorption properties of activated carbon from waste cotton textiles by FeCl3-activation. Colloids Surf, A 582:1–10. https://doi.org/10.1016/j.colsurfa.2019.123934
18. Rustamov YI, Mammadova SG, Rustamova GY, Nasirova YAG (2019) The synthesis of cellulose derivatives with special properties from cellulose- containing natural materials and priority fields of their use. 39–43
19. Herath A, Navarathna C, Warren S et al (2022) Iron/titanium oxide-biochar (Fe2TiO5/BC): a versatile adsorbent/photocatalyst for aqueous Cr(VI), Pb2+, F- and methylene blue. J Colloid Interface Sci 614:603–616. https://doi.org/10.1016/j.jcis.2022.01.067
20. Welter N, Leichtweis J, Silvestri S et al (2022) Preparation of a new green composite based on chitin biochar and ZnFe2O4 for photo-Fenton degradation of Rhodamine B. J Alloys Compounds 901:163758. https://doi.org/10.1016/j.jallcom.2022.163758
21. Wu Y, Liu B (2022) Mg(NO3)2·6H2O-modified porous carbon derived from peanut shell: formation mechanism and efficient removal of p-nitrophenol. React Kinet Mech Catal 135:2085–2098. https://doi.org/10.1007/s11144-022-02212-y
22. Zahedifar M, Seyedi N, Salajeghe M, Shafiei S (2020) Nanomagnetic biochar dots coated silver NPs (BCDs-Ag/MNPs): A highly efficient catalyst for reduction of organic dyes. Mater Chem Phys 246:122789. https://doi.org/10.1016/j.matchemphys.2020.122789
23. Lin Y, Wu S, Yang C et al (2019) Preparation of size-controlled silver phosphate catalysts and their enhanced photocatalysis performance via synergetic effect with MWCNTs and PANI. Appl Catal B Environ 245:71–86. https://doi.org/10.1016/j.apcatb.2018.12.048
24. Chen T, Luo L, Deng S et al (2018) Sorption of tetracycline on H3PO4 modified biochar derived from rice straw and swine manure. Biores Technol 267:431–437. https://doi.org/10.1016/j.biortech.2018.07.074
25. Sadeghi Rad T, Yazici ES, Khataee A et al (2023) Ultrasound-assisted photocatalytic decomposition of rifadin with biochar and CNT-based NiCr layered double hydroxides. Surf Interfaces 36:102628. https://doi.org/10.1016/j.surfin.2022.102628
26. Mohammed Dakhil R, Sumer Gaaz T, Al-Amiery A et al (2019) Synthesis and characterization of erbium trioxide nanoparticles as photocatalyzers for degradation of methyl orange dye. Drink Water Eng Sci 12:15–21. https://doi.org/10.5194/dwes-12-15-2019
27. Li Z, Hanafy H, Zhang L et al (2020) Adsorption of congo red and methylene blue dyes on an ashitaba waste and a walnut shell-based activated carbon from aqueous solutions: Experiments, characterization and physical interpretations. Chem Eng J 388:124263. https://doi.org/10.1016/j.cej.2020.124263
28. Scharte B (2010) Phosphorus-based flame retardancy mechanisms-old hat or a starting point for future development? Materials 3:4710–4745. https://doi.org/10.3390/ma3104710
29. Wei R, Cang D, Bai Y et al (2016) Reduction characteristics and kinetics of iron oxide by carbon in biomass. Ironmaking Steelmaking 43:144–152. https://doi.org/10.1179/1743281215Y.0000000061
30. Sawant SY, Munusamy K, Somani RS et al (2017) Precursor suitability and pilot scale production of super activated carbon for greenhouse gas adsorption and fuel gas storage. Chem Eng J 315:415–425. https://doi.org/10.1016/j.cej.2017.01.037
31. Alagha O, Manzar MS, Zubair M et al (2020) Magnetic Mg-Fe/LDH intercalated activated carbon composites for nitrate and phosphate removal from wastewater: insight into behavior and mechanisms. Nanomaterials 10:1–22. https://doi.org/10.3390/nano10071361
32. Mishra A, Sardar M (2015) Isolation of genomic DNA by silane-modified iron oxide nanoparticles. nanotechnology: novel perspectives and prospects. McGraw Hill Education, New York, pp 309–315
33. Gumus H, Buyükkidan B (2022) Pollution removal performance of chemically functionalized textile waste biochar anchored poly (vinylidene fluoride) adsorbent. J Turk Chem Soc Sect A Chem 9:777–792
34. Zhang L, Tu LY, Liang Y et al (2018) Coconut-based activated carbon fibers for efficient adsorption of various organic dyes. RSC Adv 8:42280–42291. https://doi.org/10.1039/c8ra08990f
35. Sartova K, Omurzak E, Kambarova G et al (2019) Activated carbon obtained from the cotton processing wastes. Diam Relat Mater 91:90–97. https://doi.org/10.1016/j.diamond.2018.11.011
36. Akinhanmi TF, Ofudje EA, Adeogun AI et al (2020) Orange peel as low-cost adsorbent in the elimination of Cd(II) ion: kinetics, isotherm, thermodynamic and optimization evaluations. Bioresour Bioprocess 7:1. https://doi.org/10.1186/s40643-020-00320-y
37. Ouedrhiri A, Ait Himi M, Youbi B et al (2022) Biochar material derived from natural waste with superior dye adsorption performance. Mater Today Proc 66:259–267. https://doi.org/10.1016/j.matpr.2022.04.928
38. Khan A, Qamar M, Muneer M (2012) Synthesis of highly active visible-light-driven colloidal silver orthophosphate. Chem Phys Lett 519–520:54–58. https://doi.org/10.1016/j.cplett.2011.11.015
39. Behrouzeh M, Mehdi Parivazh M, Danesh E et al (2022) Application of Photo-Fenton, Electro-Fenton, and Photo-Electro-Fenton processes for the treatment of DMSO and DMAC wastewaters. Arab J Chem 15:1. https://doi.org/10.1016/j.arabjc.2022.104229
40. Rauf MA, Ashraf SS (2009) Fundamental principles and application of heterogeneous photocatalytic degradation of dyes in solution. Chem Eng J 151:10–18. https://doi.org/10.1016/j.cej.2009.02.026
41. Xie G, Liu Z, Zhu Z et al (2004) Simultaneous removal of SO2 and NOx from flue gas using a CuO/Al2O3 catalyst sorbent: II Promotion of SCR activity by SO2 at high temperatures. J Catal 224:42–49. https://doi.org/10.1016/j.jcat.2004.02.016
42. Zhang L, Zou W, Ma K et al (2015) Sulfated temperature effects on the catalytic activity of CeO2 in NH3-selective catalytic reduction conditions. J Phys Chem C 119:1155–1163. https://doi.org/10.1021/jp511282c
43. Aichour A, Zaghouane-Boudiaf H, Djafer Khodja H (2022) Highly removal of anionic dye from aqueous medium using a promising biochar derived from date palm petioles: Characterization, adsorption properties and reuse studies. Arab J Chem 15:103542. https://doi.org/10.1016/j.arabjc.2021.103542
44. Luo S, Li S, Zhang S et al (2022) Visible-light-driven Z-scheme protonated g-C3N4/wood flour biochar/BiVO4 photocatalyst with biochar as charge-transfer channel for enhanced RhB degradation and Cr(VI) reduction. Sci Total Environ 806:150662. https://doi.org/10.1016/j.scitotenv.2021.150662
45. Cheng S, Zhao S, Xing B et al (2022) Preparation of magnetic adsorbent-photocatalyst composites for dye removal by synergistic effect of adsorption and photocatalysis. J Clean Prod 348:131301. https://doi.org/10.1016/j.jclepro.2022.131301

46. Park JH, Wang JJ, Meng Y et al (2019) Adsorption/desorption behavior of cationic and anionic dyes by biochars prepared at normal and high pyrolysis temperatures. Colloids Surf, A 572:274–282. https://doi.org/10.1016/j.colsurfa.2019.04.029
47. Yu F, Tian F, Zou H et al (2021) ZnO / biochar nanocomposites via solvent free ball milling for enhanced adsorption and photocatalytic degradation of methylene blue. J Hazard Mater 415:125511. https://doi.org/10.1016/j.jhazmat.2021.125511
48. Lu L, Shan R, Shi Y et al (2019) A novel TiO2/biochar composite catalysts for photocatalytic degradation of methyl orange. Chemosphere 222:391–398. https://doi.org/10.1016/j.chemosphere.2019.01.132

Authors and Affiliations

Huseyin Gumus[1] · Bulent Buyukkidan[2]

✉ Huseyin Gumus
huseyin.gumus@bilecik.edu.tr

Bulent Buyukkidan
bulent.buyukkidan@dpu.edu.tr

[1] Osmaneli Vocational School, Bilecik Seyh Edebali University, 11500 Osmaneli, Bilecik, Turkey

[2] Department of Chemistry, Kutahya Dumlupinar University, Kutahya, Turkey